Title
Design and construction of a quadruple-resonance MAS NMR probe for investigation of extensively deuterated biomolecules

Authors
Collier, Kelsey A
Sengupta, Suvrajit
Espinosa, Catalina A
et al.

Publication Date
2017-12-01

DOI
10.1016/j.jmr.2017.10.002

Peer reviewed

HHS Public Access

Author manuscript

J Magn Reson. Author manuscript; available in PMC 2019 January 03.

Published in final edited form as:

J Magn Reson. 2017 December ; 285: 8–17. doi:10.1016/j.jmr.2017.10.002.

Design and construction of a quadruple-resonance MAS NMR probe for investigation of extensively deuterated biomolecules

Kelsey A. Collier[a], **Suvrajit Sengupta**[b], **Catalina A. Espinosa**[b], **John E. Kelly**[b], **Jessica I. Kelz**[b], and **Rachel W. Martin**[b,c,*]

[a]Department of Physics & Astronomy, UC Irvine, Irvine, CA 92697-4575, United States

[b]Department of Chemistry, UC Irvine, Irvine, CA 92697-2025, United States

[c]Department of Molecular Biology & Biochemistry, UC Irvine, Irvine, CA 92697-3900, United States

Abstract

Extensive deuteration is frequently used in solid-state NMR studies of biomolecules because it dramatically reduces both homonuclear (^{1}H-^{1}H) and heteronuclear (^{1}H-^{13}C and ^{1}H-^{15}N) dipolar interactions. This approach greatly improves resolution, enables low-power rf decoupling, and facilitates ^{1}H-detected experiments even in rigid solids at moderate MAS rates. However, the resolution enhancement is obtained at some cost due the reduced abundance of protons available for polarization transfer. Although deuterium is a useful spin-1 NMR nucleus, in typical experiments the deuterons are not directly utilized because the available probes are usually triple-tuned to ^{1}H,^{13}C and ^{15}N. Here we describe a ^{1}H/^{13}C/^{2}H/^{15}N MAS ssNMR probe designed for solid-state NMR of extensively deuterated biomolecules. The probe utilizes coaxial coils, with a modified Alderman-Grant resonator for the ^{1}H channel, and a multiply resonant solenoid for ^{13}C/^{2}H/^{15}N. A coaxial tuning-tube design is used for all four channels in order to efficiently utilize the constrained physical space available inside the magnet bore. Isolation among the channels is likewise achieved using short, adjustable transmission line elements. We present benchmarks illustrating the tuning of each channel and isolation among them and the magnetic field profiles at each frequency of interest. Finally, representative NMR data are shown demonstrating the performance of both the detection and decoupling circuits.

Keywords

Solid-state NMR; Magic angle spinning; Deuterium NMR; Instrumentation; Probe development

1. Introduction

NMR structure determination requires near-complete resonance assignments and well-resolved 2D or 3D cross-peaks representing structural restraints. In solution-state NMR, ^{1}H, ^{13}C and ^{15}N chemical shifts have long been routinely used, with ^{1}H detection as the standard

*Corresponding author at: Department of Chemistry, UC Irvine, Irvine, CA 92697-2025, United States. rwmartin@uci.edu (R.W. Martin).

for many important experiments. Until the advent of fast MAS and appropriate uniform isotopic labeling schemes, the ^{1}H chemical shifts in solids had more limited value. In particular, extensive deuteration dilutes the proton spins, dramatically reducing the homonuclear (^{1}H-^{1}H) and heteronuclear (^{1}H-^{13}C and ^{1}H-^{15}N) heteronuclear dipolar interactions [1]. This improves resolution, reduces the magnitude of the rf decoupling needed, and thereby enables ^{1}H-detected experiments, even in rigid solids and at moderate MAS rates [2]. Early ^{2}H labeling schemes allowed well-resolved ^{1}H spectra to be detected even for large, complex molecules [3]. This reduction in spectral complexity was subsequently extended to ^{1}H-^{13}C and ^{1}H-^{15}N multidimensonal experiments in solution [4] and in the solid state [5]. In the most commonly used labeling scheme, the protein is expressed in D_2O, leaving all non-exchangable protons deuterated, and then back-exchanged into water [6,7]. Further recrystallization from 90% D_2O/10% H_2O yields even higher resolution [8], although there is a trade-off between resolution and sensitivity in experiments based on ^{1}H-^{13}C or ^{1}H-^{15}N cross-polarization [9], and the optimal deuteration level also depends on the MAS rate [10]. The reduction in sensitivity can be mitigated by introducing protons in random locations, which also has the advantage of providing relatively isolated protons for measurement of long-range distance restraints [11]. In sparsely protonated samples, heteronuclear dipolar couplings between ^{1}H and ^{2}H nuclei can also be measured [12]. For nanocrystalline samples, the resolution in the ^{1}H dimension of multidimensional solid-state spectra is sufficiently high to allow chemical shift assignments, as demonstrated for proteins such as ubiquitin [13,14], the SH3 domain [8], and GB1 [15]. Scalar couplings can then be straightforwardly exploited just as they are in solution-state NMR [16,17]. In non-crystalline solid-state samples, the linewidths are more variable due to dynamics and conformational exchange; however, proton-detected multidimensional experiments still assist in assignment of the backbone resonances [18]. Similarly, modified versions of widely-used homonuclear recoupling experiments (e.g. DARR/RAD [14,19] and PARIS [20]) used to measure long-range distance restraints have been developed for use in extensively deuterated proteins, where the spin dynamics, and hence the performance of recoupling sequences, are very different from those of protonated samples [21,22]. In the DOuble Nucleus Enhanced Recoupling (DONER) sequence [23] and variations thereof, both ^{1}H and ^{2}H nuclei are irradiated, using the heteronuclear interactions to recouple ^{13}C-^{13}C spin pairs.

Building on the use of deuterated samples to simplify the proton spectrum, the obvious utility of deuterium as a relatively sensitive spin-1 NMR nucleus has led to the development of pulse sequences that can be incorporated into structure determination studies. Because of the low proton abundance, polarization transfer from ^{2}H is an appealing option for fully utilizing the deuterons in multidimensional NMR. The rapid longitudinal relaxation time of the ^{2}H spins enables faster repetition rates as well as interleaved detection of signals originating on the ^{1}H and ^{2}H spins [24]. However, the magnitude of the quadrupolar interaction (on the order of 170–180 kHz) makes excitation of the entire powder pattern difficult. So far, this issue has mostly been addressed using a combination of pulse sequences and fast MAS. One approach uses a rotor-synchronized scheme designed using optimal control theory to generate efficient 90° and 180° pulses and ^{2}H-^{13}C cross-polarization [25], eliminating many of the artifacts caused by insufficient rf power. A refined

version using adiabatic pulses improves cross-polarization efficiency even with a ^{2}H rf field strength of 20 kHz [26]. Double-quantum excitation as a starting point for a multidimensional sequence allows ^{2}H to be used as a straightforward chemical shift dimension [27], and permits efficient polarization transfer with magnetization originating on the sidechains rather than a less efficient out-and-back sequence. Full assignment of the sidechain spin systems has been achieved using 2D $^{2}H_{DQ}$-^{13}C and 3D $^{2}H_{DQ}$-^{13}C-^{13}C correlation experiments [28]. Other 3D ^{2}H-^{13}C-^{13}C experiments have been used to observe site-specific side-chain dynamics which can be then correlated with biological function [29].

The rapid development of techniques incorporating ^{2}H into multi-dimensional experiments on biological macromolecules has inspired development of a dedicated quadruple-resonance MAS probe with simultaneous ^{1}H, ^{13}C, ^{2}H, and ^{15}N capability. This 4-channel MAS probe, which is optimized for detection on the lower-frequency channels, makes use of a coaxial coil design with a modified Alderman-Grant resonator on the ^{1}H channel and a variable-pitch solenoid for the three heteronuclei channels. Because this probe is intended for use with extensively deuterated samples, high-power decoupling on the proton channel is not required: we have instead optimized for sensitivity and excitation power on the heteronuclear channels. Transmission line elements are used to minimize the cross-sectional areas required by the four channels. Here we present design parameters, benchmarks, and preliminary experimental results on standard samples.

2. Probe design and mechanical implementation

2.1. Selection of coaxial coils

An NMR probe is fundamentally an LC circuit with channels that resonate at the Larmor precession frequency of each nucleus of interest. The inductance of the circuit is primarily determined by the sample coil. There are several factors that influence the choice of coil, including the efficiency of the design at the desired signal frequency and the conductive properties of the sample. Low E-field coils have long been used to avoid rf heating of conductive biological samples [30]. Their low inductance both reduces the risk of heat damage to lossy dielectric samples and makes it easier to adjust the tuning between different samples. In the context of modern multidimensional NMR, this is most important during long decoupling periods or polarization transfer pulses [31,32]. The low inductance of slotted-tube or loop-gap resonators make them most suitable for use at high frequencies, so they become more attractive options as the B_0 field strength of high-resolution NMR magnets increases. The main drawbacks of this type of coil are its comparatively lower rf power handling capabilities and its reduced sensitivity and efficiency at lower frequencies. Designs such as the scroll coil increase the sensitivity at lower frequencies, allowing multiple-resonance circuits [33,34]. The compromise in low-frequency efficiency characteristic of these low-inductance coils has also led to orthogonal or cross-coil designs utilizing coaxial coils that produce orthogonal B_1 fields. This design class is frequently used for solution-state NMR, where the vertical geometry of the coils makes it particularly convenient to implement, and in solid-state probes for static membrane samples [35,36]. However, it has also been extended to MAS probes [37]. In solids, the general principle is to make use of a wire-wound coil for the lower-frequency channels, while a low-inductance

resonator is used for the ^{1}H circuit. This design minimizes the electric field of the high-frequency channel while maximizing the sensitivity of the detection coil. In our implementation, the ^{1}H channel, which is primarily used for decoupling, makes use of a modified Alderman-Grant (MAG) resonator [38], while the ^{13}C, ^{2}H, and ^{15}N channels share a triply-tuned variable-pitch solenoid [39]. The use of a cross-coil design simplifies somewhat the complexity of the circuit required for a multiply-resonant probe. The mechanical arrangement of the two coils is shown in Fig. 1.

2.2. The ^{1}H MAG circuit

A common approach in solid-state NMR probe design is to simultaneously tune a single coil to two or three frequencies, enabling high rf power to be delivered on all channels at the expense of some reduction in sensitivity and efficiency. The circuit of each channel then contains at least two variable capacitances, one to tune the resonance frequency and the other to match the load impedance to that of the source, generally 50 Ω. Other components are added to connect the probe head to the rf amplifier and to provide isolation among the channels. This approach can be achieved using discrete circuit elements, e.g. [40,41], or transmission lines that allow tuning elements to be located far from the sample coil, e.g. [42,43].

The circuit design described here is based on the triple resonance tuning tube probe described previously [44], and incorporates a modification to the proton channel that enables all of its tune and match elements to be contained within a single vertical tube [45]. The ^{1}H circuit also contains additional elements to facilitate tuning to 800 MHz and to ensure balancing of the voltage across the sample coil. The modified Alderman-Grant coil was chosen to minimize the inductive heating of the samples. As shown in Fig. 2a the tune capacitance C_2 is divided to balance the voltage across the coil and improve B_1 homogeneity [31,46]. The tune capacitor on same side as the input rf feed is adjustable to allow tuning to the proton Larmor frequency. An adjustable match capacitance C_1 enables the impedance of the LC circuit to be matched to the input load (typically 50 Ω), minimizing reflectance. The additional inductive element L_1, in parallel with the signal coil, increases the inductance of the circuit to facilitate tuning to 800 MHz. Without L_1 the value of the tune capacitance required would be so small that the elements would be prohibitively difficult to machine using traditional methods. The small scale of the elements would also make tuning fraught with difficulty and very sensitive to temperature, such that maintaining acceptable tuning stability over the length of a multidimensional experiment would likely be difficult.

Fig. 2b shows the same circuit represented as transmission line segments. These coaxial elements can be contained within an external ground shield, allowing the channels of the probe to be packed together in the two-inch diameter of the magnet bore.

2.3. The ^{13}C/^{2}H/^{15}N triple-tuned solenoid circuit

The variable pitch solenoid was chosen for this circuit because this design is simple and provides good efficiency and sensitivity at the relevant frequencies. The solenoid circuit consists of the tune and match elements required to resonate at the Larmor frequency of each

nucleus, as well as several isolation elements to minimize interference among the three channels that share the coil.

The solenoid circuit is shown in Fig. 3 using transmission line notation. Each channel is contained within a grounded cylindrical shield in order to minimize stray reactances. C_1, C_3 and C_9 are the match capacitors and C_2, C_4 and C_{10} are the tune capacitors of the ^{13}C, ^{2}H, and ^{15}N channels, respectively. Other circuit elements provide isolation among the channels and assist with tuning. Elements C_8 and L_8 make up a parallel resonant trap tuned to the ^{2}H frequency to isolate the ^{15}N channel. The ^{13}C channel is connected in parallel to an isolation element, capacitance C_5 in series with the parallel circuit of capacitance C_6 and inductance L_6 created by a shorted 1/4-wavelength transmission line segment. This isolation element functions as a low-frequency path to ground, isolating ^{13}C from the lower-frequency channels.

The versatility of transmission line segments in high-frequency circuits can be seen in Fig. 3. Transmission line segment reactance in high-frequency rf circuits is sensitive to the length of the segment relative to the wavelength of the signal. Segments much shorter than the wavelength of the signal behave purely capacitively (open) or inductively (shorted), allowing them to be used as discrete circuit elements [47]. Open or shorted quarter-wavelength segments behave as a low- or high-impedance resonant circuits, respectively, allowing them to be used as isolation elements.

2.4. Tuning tube geometry

One major challenge in fabricating the quadruple-resonance MAS probe is fitting all the required circuit components, air lines, variable-temperature dewar, structural support, and magic-angle adjust within the two-inch diameter of the magnet bore. In the tuning tube design, the tune and match network of each channel is composed of coaxial elements, allowing the circuit elements to be distributed over the length of the probe and thereby making efficient use of the available volume. These coaxial capacitors are physically robust, with good power handling capabilities and reasonable tunability at high frequencies. This coaxial design enables each rf channel to be placed in a cylindrical grounded shield, eliminating many sources of stray reactances, which are a major concern in a high-frequency multi-channel probe.

Fig. 4a shows a schematic of the top plate of the probe frame, illustrating the significant spatial constraints of the circuit and associated components. Fig. 4b shows a schematic of the probe-head and the tight spacial constraints on the arrangement of the leads.

These space constraints also apply to the components within each channel; the nested cylindrical components of the design minimize the required cross-sectional area of each channel. The channel layouts are depicted in Fig. 5; a common design is used for the ^{2}H, ^{13}C, and ^{15}N channels (Fig. 5a and b), while the ^{1}H channel incorporates an additional grounded transmission line segment to facilitate tuning to 800 MHz (Fig. 5c). Fig. 5b shows a cross-section of the low-frequency channels. The dimensions depicted are for ^{13}C at 200 MHz; dimensions of the critical components for all three channels are given in Table 1. Starting near the bottom of the diagram, the rf signal from the spectrometer enters the probe

circuit via a coaxial line. This is accomplished using a type-N quick-change connector (Bird Electronics, Solon, OH) that makes contact by pressing into a boss soldered onto the 1/4 OD center conductor of the match feed. This line acts as an air dielectric capacitor with 3/4'' OD (the outer cylinder of the channel) and ¼'' ID (the match feed cylinder) over most of the length of the probe, serving to capacitively connect the rf input to the matching network. The value of the coupling capacitance between the rf feed and the match element is not critical.

The lower part of the match element consists of a 1/8'' diameter copper rod tightly covered by Teflon dielectric such that it slides freely in and out of the top of the center conductor. The upper part of the match element is a larger copper cylinder terminated with a hemispherical end, encased within a Teflon sleeve with a corresponding hemispherical pocket. The base of this larger cylinder must also be ground down to a curve where it meets the lower match element. These features are required in order to prevent the corona discharge and eventual dielectric breakdown that otherwise results from having sharp edges and/or air pockets at this high-voltage point in the circuit. The entire assembly comprising the upper match conductor and its dielectric cover fits into a hemispherical pocket in the copper tune conductor cylinder. The inner plate of the match capacitor is the surface of this upper match element; the outer plate is the interior surface of the tune conductor. The value of the match capacitance is adjusted by moving the match conductor up and down within the cavity of the tune conductor. This linear motion is actuated using the match adjust knob (shown in the lower inset). The rotational motion of the knob is transformed into linear motion by a captured thread. The end of the rf connector fits into a machined slot in the central match guide rod, preventing this rod from turning. Backlash in this mechanism should be minimized, because the probe matching is very sensitive to small movements of this circuit element.

The tune center conductor, which is capacitively coupled to the match as described above, consists of a copper cylinder with a hollow chamber which the match element is inserted into. The tune center conductor is surrounded by a hollow Teflon dielectric cylinder which can be moved vertically, allowing the tune capacitance to be adjusted. The inner plate of the tune capacitor is the outer surface the tune center conductor; the outer plate of this cylindrical capacitor is the inner surface of the grounded outer tube enclosing the channel. Maximum capacitance, and hence the lowest frequency, is achieved by maximizing the overlap between the Teflon dielectric and the center conductor. The minimum capacitance (highest frequency) occurs when the cylinder is fully retracted, making the tune capacitor fully air dielectric. The top of the center conductor has a stub allowing a lead to be connected to the coil. At the top of the channel, a tight Teflon plug is press-fit into the tube in order to keep the tune center conductor from falling into the tube or being pushed out of it. The capacitance generated by this fixed top plug is not critical, but it is significant enough that it should be accounted for in simulations of the circuit. The adjustable tune dielectric is connected to the tune knob by two 1/8''Delrin guide rods pressed into slots in a Delrin actuator at the bottom and secured by copper wire pins. A brass key attached to the outer knob housing slides into a slot machined into the tune actuator to prevent rotation of this assembly. The guide rods are prevented from turning by Teflon spacers located at intervals along the length of the center conductor. Without the key and spacers, backlash in the mechanism causing uncontrolled motions of the dielectric is a significant problem that

impacts the tuning reproducibility. It is also essential to place thin Teflon washers between all the rotating brass pieces in the knob assembly in order to prevent sticking of the tune and match knobs.

In all cases, the match guide rods are machined from Delrin with an outer diameter of 3/16'' and the tune guide rods from Delrin with an outer diameter of 0:125''.

As shown in Fig. 5b, the proton channel has a similar design. The additional inductive element required to tune at high frequency alters the configuration at the top of the channel, and the smaller dimensions of the tuning elements allow the circuit to be contained in an outer tube with a diameter of 0:625''. The rf signal is fed from a Type-N quick-change connector to a coaxial line. The bottom end of the moveable match element, a 1/8'' diameter copper rod covered with Teflon tubing, is inserted into the top of this center conductor. This is where the divergence in design from the heteronuclei channels begins. This lower rod of the moveable match element has a small rectangular plate (0.2″″× 0.5'') soldered across the top. Two copper wires, each covered for most of their 2'' length with thin Teflon tubing, extend up from the plate to a thin copper cylinder, anchored by solder joints on both ends. This thin cylinder (OD 0:29'', ID 0:27'') forms the upper match conductor, with a capacitance to the tune center conductor. The additional inductance required for tuning is provided by a transmission line segment formed by a short (0:25'') cylinder soldered to the base of the tune center conductor. The outside of this cylinder (OD 0:55'') is grounded by two screws passing through the outer tube of the channel. The upper portion of the match assembly is located above the inductive stub; the two wire connectors pass through holes drilled in its cylinder. Care must be taken with the length of these wires and the match guide rod to allow the range of motion needed to properly adjust the match capacitance. Tune adjustment is again accomplished through vertical motion of a dielectric cylinder.

3. Benchmarking and experimental results

Reflectances were measured on an Agilent Technologies E5061A Network Analyzer to verify the tuning of each channel (Fig. 6). All four channels were tuned simultaneously for this measurement. In each case the impedance matching is better than 60 dB.

Minimizing interference among the heteronuclear channels using isolation elements is an important aspect of the design shown in Fig. 3. The isolation between each set of channels was measured by sweeping the input frequency of one channel and detecting on another, using an Agilent Technologies E5061A Network Analyzer. Ideally the signal should be minimized at the tuning frequency of the detection channel. The isolation output for all three combinations of channels on the solenoid circuit is shown in Fig. 7.

The isolation values at the signal frequencies are reported below in Table 2. Isolation measurements were performed on the heteronuclear channels that share the solenoid coil.

The coaxial coil design requires careful alignment of the homogeneous region of the magnetic field of each coil to enable maximum efficiency in cross-polarization and decoupling. For each coil, the magnetic field profile was measured with the ball-shift method, in which the change in resonant frequency is measured as a small copper disc is

moved through the coils on a finely threaded rod [46]. Fig. 8 shows the magnitude of the frequency shift as a function of longitudinal displacement along the coils for each frequency of interest. It is readily seen that the circuits are balanced, and the homogeneous region of the solenoid coil and the modified Alderman-Grant resonator largely overlap each other.

4. Spectrometer testing

All experiments were performed in an 18.8 Tesla (799.8 MHz in ^{1}H Larmor frequency) Oxford superconducting magnet equipped with a Varian $^{\text{UNITY}}$INOVA spectrometer console. The console was controlled by a Dell Z420 Workstation running Agilent VnmrJ 4.2 software. Pulse power levels were calculated from peak-to-peak voltages measured through a 50 dB attenuated directional coupler on a Tektronix TDS5104B digital oscilloscope and a reported in Table 3. The reported Q-values of the channels were calculated from the measured reflectances in Fig. 6, and are given by the equation:

$$Q=\frac{2\omega_0}{\Delta\omega}$$

where ω_0 is the resonance frequency of the channel and is $\Delta\omega$ the width of the response at −3 dB from the baseline.

Nutation curves (Fig. 9) provide a good indication of the rf homogeneity and efficiency. The ^{1}H and ^{13}C nutation curves were recorded using a one pulse experiment on a natural abundance adamantane sample. The ^{2}H nutation was recorded using a one pulse experiment on a sample containing 90% D_2O/10% H_2O. The ^{15}N nutation was recorded with an ^{1}H-^{15}N cross-polarization experiment (see below) on an L-Alanine-$^{13}C_3$, ^{15}N sample. Probe manufacturers often quote the ratio of signal intensity after an 810° pulse to that after a 90° pulse as a measure of the efficiency of the probe. The 90°-times and 810°/90° ratios for the probe are reported in Table 3. The quoted power levels are tolerated by the probe for long pulses without arcing. The use of a low-inductance transverse coil for the ^{1}H channel reduces its maximum rf power tolerance relative to a solenoid. However, since the focus here is on deuterated samples, high-power ^{1}H decoupling is not required and the coil is only required to deliver a sufficient field for cross-polarization. The planned future generations of this probe will use of 2 mm or 1.6 mm rotors, so that the ultra-fast MAS and low-power decoupling schemes that have been successful in many protein systems [48–51] may be used.

The cross-polarization (CP) match conditions were determined for the ^{13}C and ^{15}N channels. The ^{1}H-^{13}C CP experiment was conducted on a natural abundance adamantane sample spinning at ~9 kHz. A CP contact time of 1 ms was used. The ^{13}C CP pulse was kept constant at a B_1 field strength of 17.5 kHz, while the ^{1}H pulse was varied. With the Hartmann-Hahn matching condition defined as ω_1H ω_X $n+\omega_r$, where ω_{1H} and ω_X are the B_1 fields in hertz during the CP pulse of the ^{1}H and X channels respectively, and ω_r is the rotor frequency in hertz, the match conditions are obtained for n = +1 and +2, as shown in Fig. 10a. The ^{1}H-^{15}N CP experiment was conducted on an L-Alanine-$^{13}C_3$; ^{15}N sample spinning at ~12 kHz. A CP contact time of 250 μs was used. The ^{1}H CP pulse was kept

constant at a B_1 field strength of 40 kHz, while the ^{15}N pulse was varied. The match conditions are obtained for $n = +1$ and +2, as shown in Fig. 10b. Fig. 10c shows a ^{1}H-^{13}C HET-COR spectrum of natural abundance adamantane, where the ^{1}H chemical shift was evolved during the F_1 and then the magnetization was transferred to ^{13}C using the +1 CP match condition and then detected directly during F_2.

Solid-state ^{2}H NMR experiments were conducted on an L-Alanine-$^{13}C_3$, ^{15}N,2,3,3,3-d_4 sample (Sigma-Aldrich). A solid echo sequence with an echo delay of 100μs was used to acquire the deuterium spectra. Fig. 11a shows the static spectrum acquired with 1024 scans with a recycle delay of 500 ms. As can be seen from the figure, the quadrupolar lineshape is preserved and the entire width of the powder pattern for this sample can be excited in our probe. Fig. 11b shows the MAS spinning spectrum with the sample spinning at ~9 kHz. The envelope of the spinning side-bands reproduces the static line shape. In addition, the presence of two slightly different quadrupolar interactions arising from the two chemically distinct ^{2}H species can be discerned.

5. Conclusion

Introducing deuterium excitation and detection will greatly expand the range of techniques available for solid and semi-solid samples, enabling the type of exquisitely sensitive ^{2}H-based measurements of local order parameters, orientation, and mobility currently available in liquids or liquid crystals. New experiments such as ^{2}H-^{13}C and ^{2}H-^{15}N correlations will also provide an additional degree of freedom for structural studies. Our four-channel probe can detect or decouple any combination of ^{1}H, ^{13}C, ^{2}H, and ^{15}N, although it is optimized for detection on the lower-frequency channels. Future variants will explore the possibilities afforded by fast MAS and proton detection.

Acknowledgement

This research was supported by NIH grant 1R01 EY021514 to RWM. JIK acknowledges support from NIH grant T32 GM108561. The authors thank Hartmut Oschkinat, Ümit Akbey, and Chad Rienstra for insightful discussions and Ilya Litvak for his gift of the Pd-plated Cu zero susceptibility wire.

References

[1]. Crespi HL, Rosenberg RM, Katz JJ, Proton magnetic resonance of proteins fully deuterated except for ^{1}H-Leucine side chains, Science 161 (1968) 795–796. [PubMed: 5663808]

[2]. Hologne M, Faelber K, Diehl A, Reif B, Characterization of dynamics of perdeuterated proteins by MAS solid-state NMR, J. Am. Chem. Soc 127 (32) (2005) 11208–11209. [PubMed: 16089426]

[3]. LeMaster DM, Richards FM, NMR sequential assignment of *Escherichia coli* thioredoxin utilizing random fractional deuteration, Biochemistry 27 (1988) 142–150. [PubMed: 3280013]

[4]. Gardner KH, Kay LE, The use of ^{2}H, ^{13}C, ^{15}N multidimensional NMR to study the structure and dynamics of proteins, Annu. Rev. Biophys. Biomol. Struct 27 (1) (1998) 357–406. [PubMed: 9646872]

[5]. Hologne M, Chevelkov V, Reif B, Deuterated peptides and proteins in MAS solid-state NMR, Prog. Nucl. Magn. Reson. Spectrosc 48 (2006) 211–232.

[6]. Lemaster DM, Deuteration in protein proton magnetic resonance, Methods Enzymol 177 (1989) 23–43. [PubMed: 2607981]

[7]. Sattler M, Fesik SW, Use of deuterium labeling in NMR: overcoming a sizeable problem, Structure 4 (1996) 1245–1249. [PubMed: 8939758]

[8]. Chevelkov V, Rehbein K, Diehl A, Reif B, Ultrahigh resolution in proton solid-state NMR spectroscopy at high levels of deuteration, Angew. Chem. Int. Ed 45 (23) (2006) 3878–3881.

[9]. Akbey U, Lange S, Franks WT, Linser R, Rehbein K, Diehl A, van Rossum B, Reif B, Oschkinat H, Optimum levels of exchangeable protons in perdeuterated proteins for proton detection in MAS solid-state NMR, J. Biomol. NMR 46 (2010) 67–73. [PubMed: 19701607]

[10]. Nieuwkoop AJ, Franks WT, Rehbein K, Diehl A, Akbey Ü, Engelke F, Emsley L, Pintacuda G, Oschkinat H, Sensitivity and resolution of proton detected spectra of a deuterated protein at 40 and 60 kHz magic-angle-spinning, J. Biomol. NMR 61 (2015) 161–171. [PubMed: 25663049]

[11]. Asami S, Reif B, Proton-detected solid-state NMR spectroscopy at aliphatic sites: application to crystalline systems, Acc. Chem. Res 46 (9) (2013) 2089–2097. [PubMed: 23745638]

[12]. Karki I, Mihaliuk E, Gullion T, ^{1}H-observe ^{1}H-^{2}H dipolar recoupling by REDOR and rotary resonance recoupling, Isr. J. Chem 54 (1–2) (2014) 163–170.

[13]. Paulson EK, Morcombe CR, Gaponenko V, Dancheck B, Byrd RA, Zilm KW, Sensitive high-resolution inverse detection NMR spectroscopy of proteins in the solid state, J. Am. Chem. Soc 125 (2003) 15831–15836. [PubMed: 14677974]

[14]. Morcombe CR, Gaponenko V, Byrd RA, Zilm KW, Diluting abundant spins by isotope edited radio frequency field assisted diffusion, J. Am. Chem. Soc 126 (2004) 7196–7197. [PubMed: 15186155]

[15]. Zhou D, Graesser DT, Franks WT, Rienstra CM, Sensitivity and resolution in proton solid-state NMR at intermediate deuteration levels: quantitative linewidth characterization and applications to correlation spectroscopy, J. Magn. Reson 178 (2006) 297–307. [PubMed: 16289756]

[16]. Linser R, Fink U, Reif B, Proton-detected scalar coupling based assignment strategies in MAS solid-state NMR spectroscopy applied to perdeuterated proteins, J. Magn. Reson 193 (1) (2008) 89–93. [PubMed: 18462963]

[17]. Barbet-Massin E, Pell AJ, Jaudzems K, Franks WT, Retel S, Joren S Svetlana KotelovicaInara Akopjana, K. Tars, L. Emsley, H. Oschkinat, A. Lesage, G. Pintacuda, Out-and-back ^{13}C–^{13}C scalar transfers in protein resonance assignment by proton-detected solid-state NMR under ultra-fast MAS, J. Biomol. NMR 56 (4) (2013) 379–386. [PubMed: 23812971]

[18]. Linser R, Dasari M, Hiller M, Higman V, Fink U, Lopez Del Amo JM, Markovic S, Handel L, Kessler B, Schmieder P, Oesterhelt D, Oschkinat H, Reif B, Proton-detected solid-state NMR spectroscopy of fibrillar and membrane proteins, Angew. Chem. Int. Ed 50 (19) (2011) 4508–4512.

[19]. Takegoshi K, Nakamura S, Terao T, ^{13}C–^{1}H dipolar-assisted rotational resonance in magic-angle spinning NMR, Chem. Phys. Lett 344 (2001) 631–637.

[20]. Weingarth M, Demco D, Bodenhausen G, Tekely P, Improved magnetization transfer in solid-state NMR with fast magic angle spinning, Chem. Phys. Lett 469 (2009) 342–348.

[21]. Huang K-Y, Siemer AB, McDermott AE, Homonuclear mixing sequences for perdeuterated proteins, J. Magn. Reson 208 (2011) 122–127. [PubMed: 21094063]

[22]. Akbey Ü, van Rossum BJ, Oschkinat H, Practical aspects of high-sensitivity multidimensional ^{13}C MAS NMR spectroscopy of perdeuterated proteins, J. Magn. Reson 217 (2012) 77–85. [PubMed: 22440428]

[23]. Akbey Ü, Oschkinat H, Van Rossum BJ, Double-nucleus enhanced recoupling for efficient ^{13}C MAS NMR correlation spectroscopy of perdeuterated proteins, J. Am. Chem. Soc 131 (2009) 17054–17059. [PubMed: 19929015]

[24]. Bjerring M, Paaske B, Oschkinat H, Akbey Ü, Nielsen NC, Rapid solid-state NMR of deuterated proteins by interleaved cross-polarization from ^{1}H and ^{2}H nuclei, J. Magn. Reson 214 (2012) 324–328. [PubMed: 22130517]

[25]. Wei D, Akbey U, Paaske B, Oschkinat H, Reif B, Bjerring M, Nielsen NC, Optimal ^{2}H rf pulses and ^{2}H^{13}C cross-polarization methods for solid-state ^{2}H MAS NMR of perdeuterated proteins, J. Phys. Chem. Lett 2 (2011) 1289–1294. [PubMed: 26295423]

[26]. Jain SK, Nielsen AB, Hiller M, Handel L, Ernst M, Oschkinat H, Akbey Ü, Nielsen NC, Low-power polarization transfer between deuterons and spin-1/2 nuclei using adiabatic (RESPIRATION)CP in solid-state NMR, Phys. Chem. Chem. Phys. Chem. Chem. Phys 16 (7) (2014) 2827–2830. [PubMed: 24418905]

[27]. Agarwal V, Diehl A, Skrynnikov N, Reif B, High-resolution ^{1}H detected $^{1}H,^{13}C$ correlation spectra in MAS solid-state NMR using deuterated proteins with selective $^{1}H,^{2}H$ isotopic labeling of methyl groups, J. Am. Chem. Soc 128 (39) (2006) 12620–12621. [PubMed: 17002335]

[28]. Lalli D, Schanda P, Chowdhury A, Retel J, Hiller M, Higman VA, Handel L, Agarwal V, Reif B, Van Rossum B, Akbey Ü, Oschkinat H, Three-dimensional deuterium-carbon correlation experiments for high-resolution solid-state MAS NMR spectroscopy of large proteins, J. Biomol. NMR 51 (4) (2011) 477–485. [PubMed: 22038621]

[29]. Shi X, Rienstra CM, Site-specific internal motions in GB1 protein microcrystals revealed by 3D $^{2}H^{13}C^{13}C$ solid-state NMR spectroscopy, J. Am. Chem. Soc 138 (12) (2016) 4105–4119. [PubMed: 26849428]

[30]. Alderman DW, Grant DM, An efficient decoupler coil design which reduces heating in conductive samples in superconducting spectrometers, J. Magn. Reson 36 (3) (1979) 447–451.

[31]. Doty FD, Kulkarni J, Turner C, Entzminger G, Bielecki A, Using a cross-coil to reduce RF heating by an order of magnitude in triple-resonance multinuclear MAS at high fields, J. Magn. Reson 182 (2) (2006) 239–253. [PubMed: 16860580]

[32]. Gor'kov PL, Chekmenev EY, Li C, Cotten M, Buffy JJ, Traaseth NJ, Veglia G, Brey WW, Using low-E resonators to reduce RF heating in biological samples for static solid-state NMR up to 900 MHz, J. Magn. Reson 185 (1) (2007) 77–93. [PubMed: 17174130]

[33]. Stringer JA, Bronniman CE, Mullen CG, Zhou DH, Stellfox SA, Li Y, Williams EH, Rienstra CM, Reduction of RF-induced sample heating with a scroll coil resonator structure for solid-state NMR probes, J. Magn. Reson 173 (2005) 40–48. [PubMed: 15705511]

[34]. Grant CV, Sit SL, De Angelis AA, Khuong KS, Wu CH, Plesniak LA, Opella SJ, An efficient H-1/P-31 double-resonance solid-state NMR probe that utilizes a scroll coil, J. Magn. Reson 188 (2007) 279–284. [PubMed: 17719813]

[35]. Gor'kov PL, Witter R, Chekmenev EY, Nozirov F, Fu R, Brey WW, Low-E probe for ^{19}F-^{1}H NMR of dilute biological solids, J. Magn. Reson 189 (2) (2007) 182–189. [PubMed: 17920316]

[36]. Grant CV, Yang Y, Glibowicka M, Wu CH, Park SH, Deber CM, Opella SJ, A modified Alderman-Grant coil makes possible an efficient cross-coil probe for high field solid-state NMR of lossy biological samples, J. Magn. Reson 201 (1) (2009) 87–92. [PubMed: 19733108]

[37]. McNeill SA, Gor'kov PL, Shetty K, Brey WW, Long JR, A low-E magic angle spinning probe for biological solid state NMR at 750 MHz, J. Magn. Reson 197 (2) (2009) 135–144. [PubMed: 19138870]

[38]. Grant CV, Wu CH, Opella SJ, Probes for high field solid-state NMR of lossy biological samples, J. Magn. Reson 204 (2) (2010) 180–188. [PubMed: 20435493]

[39]. Idziak S, Haeberlen U, Design and construction of a high homogeneity rf coil for solid-state multiple-pulse NMR, J. Magn. Reson 288 (1982) 281–288.

[40]. Cross VR, Hester RK, Waugh JS, Single coil probe with transmission-line tuning for nuclear magnetic double-resonance, Rev. Sci. Instrum 47 (1976) 1486–1488.

[41]. Kan S, Fan M, Courtieu J, A single-coil triple resonance probe for NMR experiments, Rev. Sci. Instrum 51 (7) (1980) 887–890.

[42]. McKay R, Probes for special purposes, Encyclopedia Magn. Reson 6 (1996) 3768–3771.

[43]. Barnes AB, Mak-Jurkauskas ML, Matsuki Y, Bajaj VS, van der Wel R, Patrick CA DeRocher, Bryant J, Sirigiri JR, Temkin RJ, Lugtenburg J, Herzfeld J, Griffin RG, Cryogenic sample exchange NMR probe for magic angle spinning dynamic nuclear polarization, J. Magn. Reson 198 (2009) 261–270. [PubMed: 19356957]

[44]. Martin RW, Paulson EK, Zilm KW, Design of a triple resonance magic angle sample spinning probe for high field solid state nuclear magnetic resonance, Rev. Sci. Instrum 74 (6) (2003) 3045–3061.

[45]. Paulson EK, Hardware and Methods Development for Protein Structure Elucidation by Solid-state NMR Spectroscopy Ph.D. thesis, Yale University, 2004.

[46]. Paulson EK, Martin RW, Zilm KW, Cross polarization, radio frequency field homogeneity, and circuit balancing in high field solid state NMR probes, J. Magn. Reson 171 (2) (2004) 314–323. [PubMed: 15546758]

[47]. Terman FE, Resonant lines in radio circuits, Electr. Eng 53 (7) (1934) 1046–1053.

[48]. Ishii Y, Yesinowski JP, Tycko R, Sensitivity enhancement in solid-state C-13 NMR of synthetic polymers and biopolymers by H-1 NMR detection with high-speed magic angle spinning, J. Am. Chem. Soc 123 (2001) 2921–2922. [PubMed: 11456995]

[49]. Zhou DH, Shah G, Cormos M, Mullen C, Sandoz D, Rienstra CM, Proton-detected solid-state NMR spectroscopy of fully protonated proteins at 40 kHz magic-angle spinning, J. Am. Chem. Soc 129 (2007) 11791–11801. [PubMed: 17725352]

[50]. Laage S, Marchetti A, Sein J, Pierattelli R, Sass HJ, Grzseiek S, Lesage A, Pintacuda G, Emsley L, Band-selective ^{1}H-^{13}C cross-polarization in fast magic angle spinning solid-state NMR spectroscopy, J. Am. Chem. Soc 130 (2008) 17216–17217. [PubMed: 19053413]

[51]. Salager E, Stein RS, Steuernagel S, Lesage A, Elena B, Emsley L, Enhanced sensitivity in high-resolution ^{1}H solid-state NMR spectroscopy with DUMBO dipolar decoupling under ultra-fast MAS, Chem. Phys. Lett 469 (2009) 336–341.

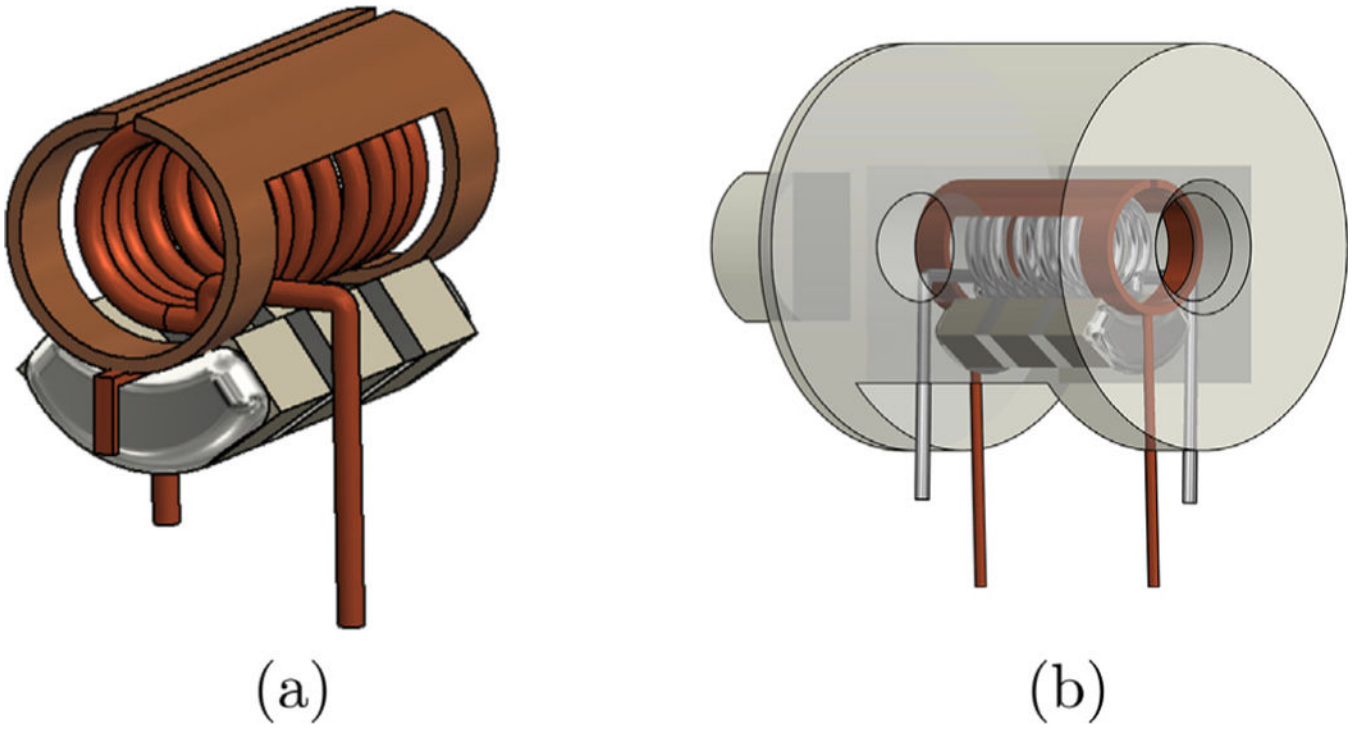

Fig. 1.

Diagram of the coaxial coils (a) outside and (b) inside the stator, which was purpose-built by Revolution NMR (Fort Collins, CO). The outer (^{1}H) coil is a modified Alderman-Grant resonator, while the inner coil (^{13}C, ^{2}H, ^{15}N) is a variable-pitch solenoid. The MAG resonator is machined from a 0:25'' OD OFHC tube, drilled out to ID 0:199''. The resonator is 0:5'' with the window having a length of 0:3'' and the tab a width of 0:1607''. The capacitive bridge is made of a 2 × 2 arrangement of 3.3 pF high-Q ceramic chip capacitors from Johanson Technology (Camarillo, CA). The six-turn solenoid is wound from 22 gauge Pd plated Cu wire (diameter 0:0254'') to an inner diameter of 0:142''.

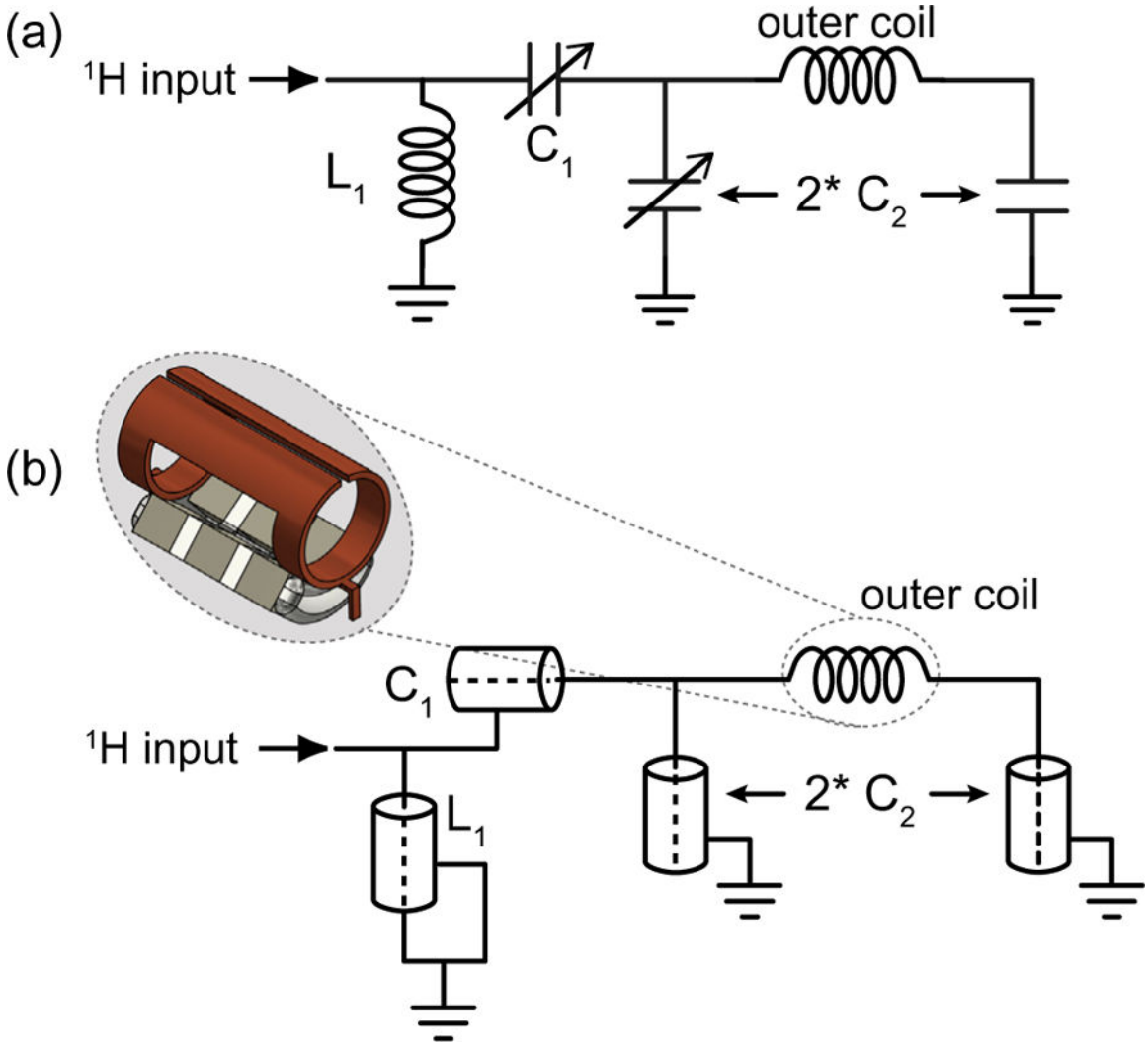

Fig. 2.

(a) Discrete-element circuit diagram of the ^{1}H channel. The match capacitance is C_1; the tune capacitance C_2 is split across the resonator. The additional inductive element L_1 is necessary for tuning to high frequency. (b) The tuning tube (transmission line element) notation is equivalent, but more accurately depicts the physical construction of the circuit. Dashed lines indicate the central coaxial element of the tuning tube segments, while the solid lines indicate the outer cylinder. Also shown is an illustration of the modified Alderman-Grant coil.

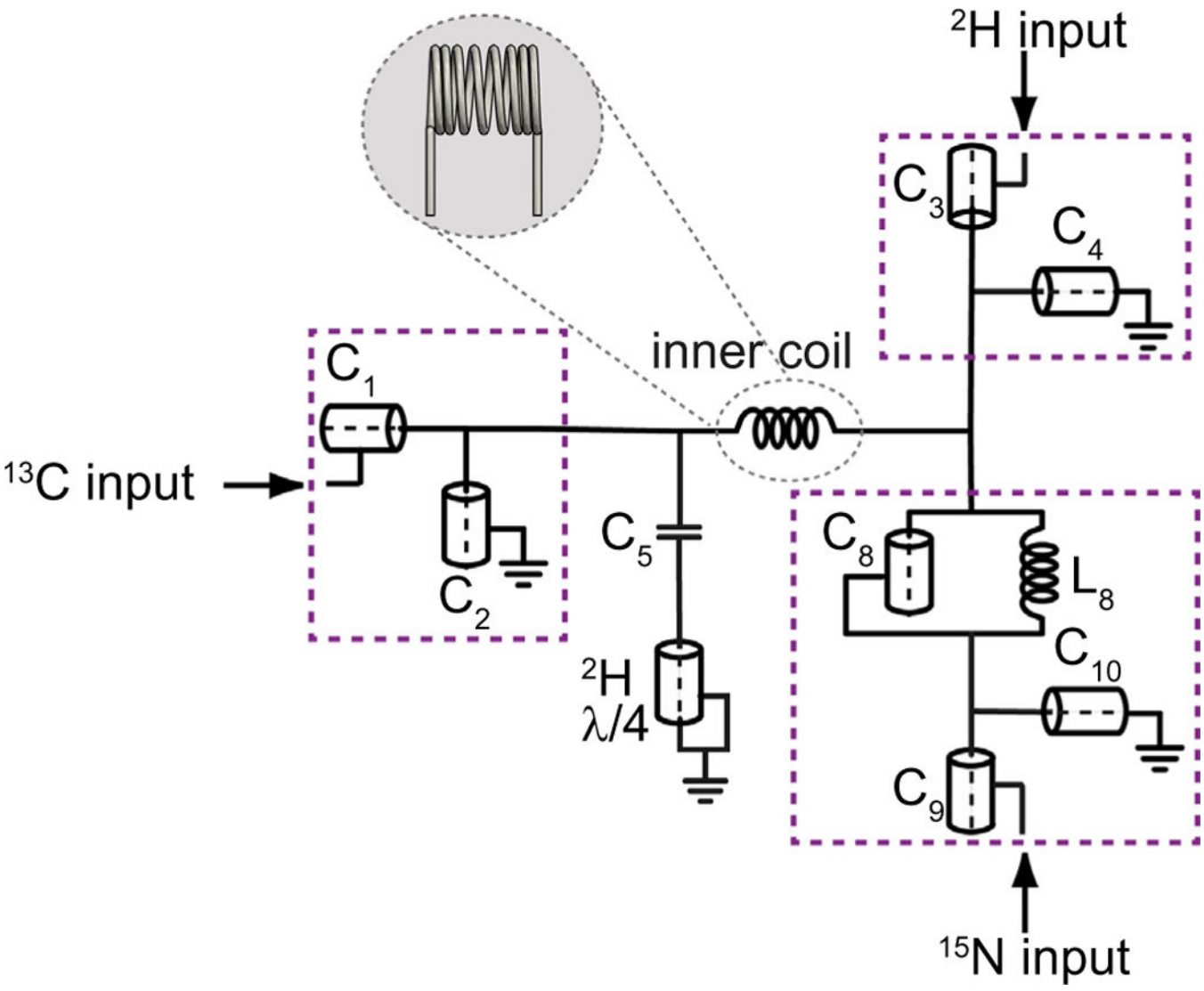

Fig. 3.

The $^{13}C/^{2}H/^{15}N$ circuit makes use of a triple-tuned solenoid. Matching is accomplished with variable capacitances C_1, C_3 and C_9 and tuning with variable capacitances C_2, C_4 and C_{10}. Isolation is provided by C_8 and L_8 and C_5, C_6 and L_6. The purple boxes indicate the subcircuit ‘‘channels” that contain the circuit elements for each of the heteronuclei, each of which is contained in a grounded outer cylinder. All circuit elements are composed of transmission line segments except for *C*5, which is a commercial chip capacitor, and *L*8, which is a hand-wound variable-pitch solenoid. Also shown is an illustration of the actual variable-pitch solenoid coil.

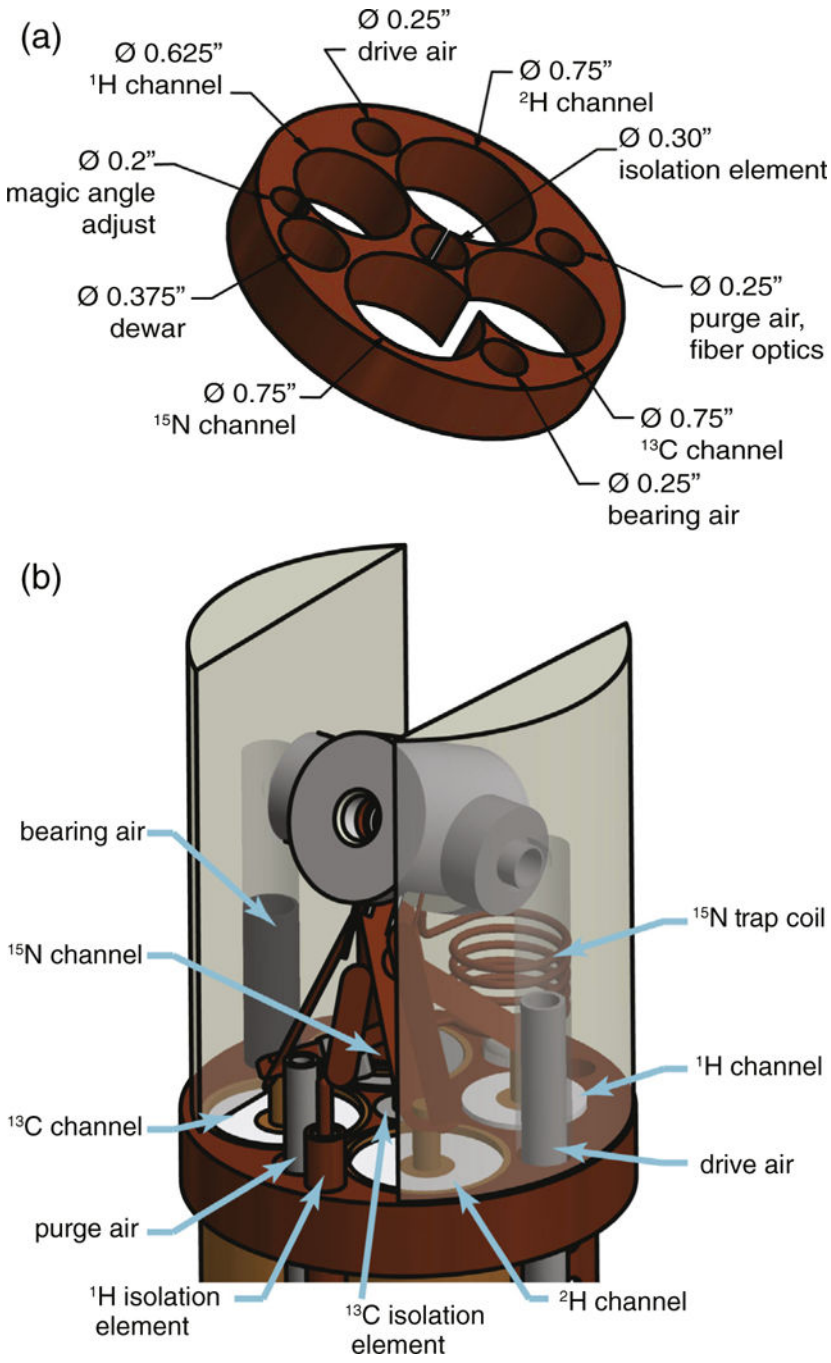

Fig. 4.

(a) Mechanical drawing of the top plate of the 4-channel probe, showing the positioning of channel circuits, air lines, and mechanical support structures. Containing the rf circuit of each channel in its own grounded cylinder allows the channels to be tightly packed. (b) Schematic of the probehead. The stator supports have been made translucent in the drawing to allow greater visibility. Care must be taken with the arrangement of the leads in the small volume.

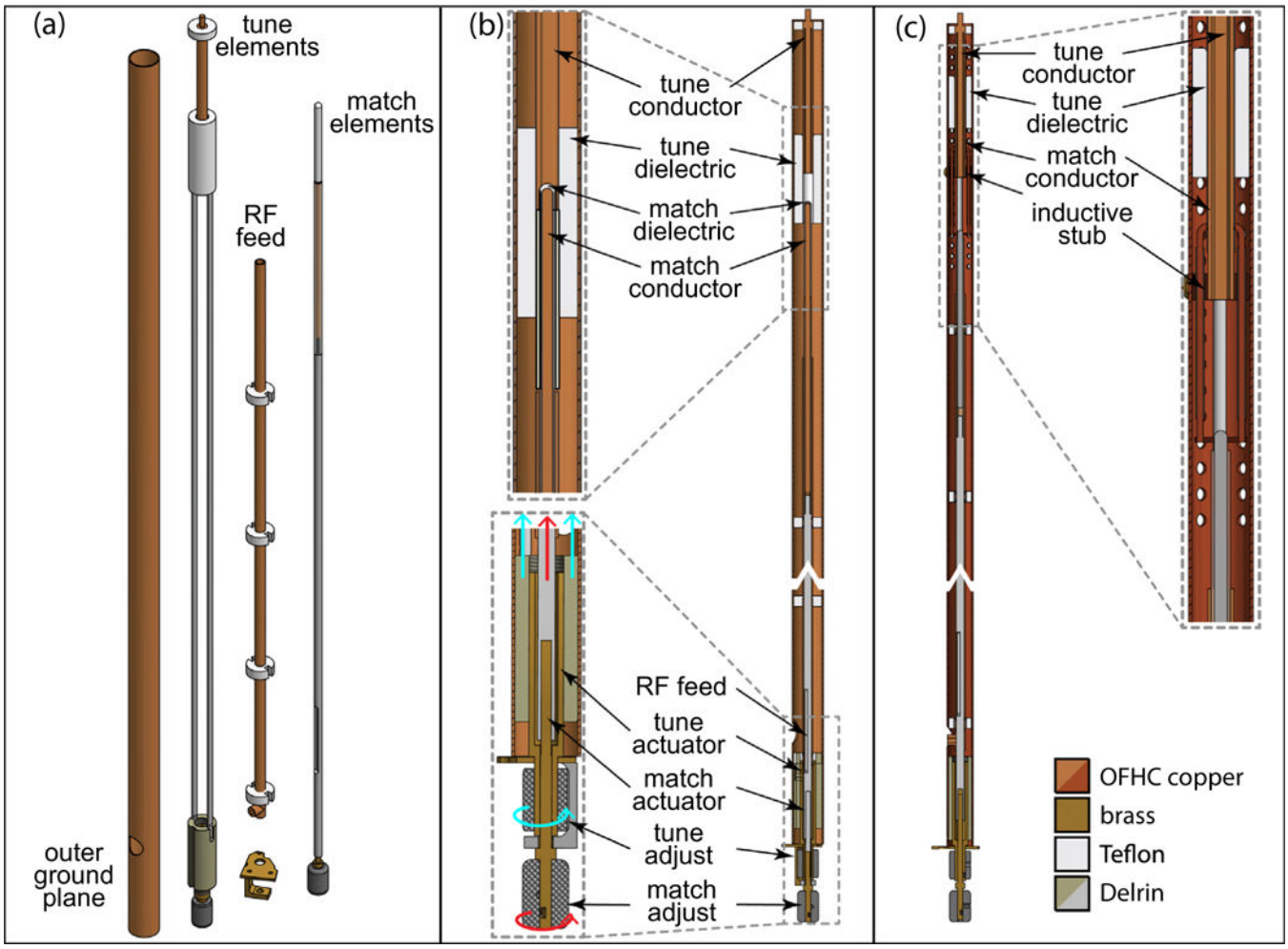

Fig. 5.

(a) Exploded view of a heteronuclear channel illustrating the concentric design. (b) A cross-section of one of the heteronuclear channels. The coaxial properties of transmission line segments allow the components of the tune and match capacitances to be arranged concentrically. The rf input from the spectrometer is connected through a type-N connector to the rf feed at the bottom of the channel, capacitively coupled to the match conductor, then to the tune conductor, from which a ribbon lead goes to the coil. The knobs at the bottom of the channel rotate actuators that, via threaded rods that run the length of the probe, adjust the vertical position of the match conductor (motion indicated by red arrows) and the tune dielectric cylinder (motion indicated by blue arrows), thereby controlling the match and tune capacitances. (c) A cross-section of the ^{1}H channel. The inductive stub used to tune at high frequency requires a different geometry for the match capacitance from the heteronuclei case. The control of the tuning and matching is accomplished in the same manner. (The cross-hatched elements in the figure b and c indicate the outer ground plane of the channel.). (For interpretation of the references to colour in this figure legend, the reader is referred to the web version of this article.)

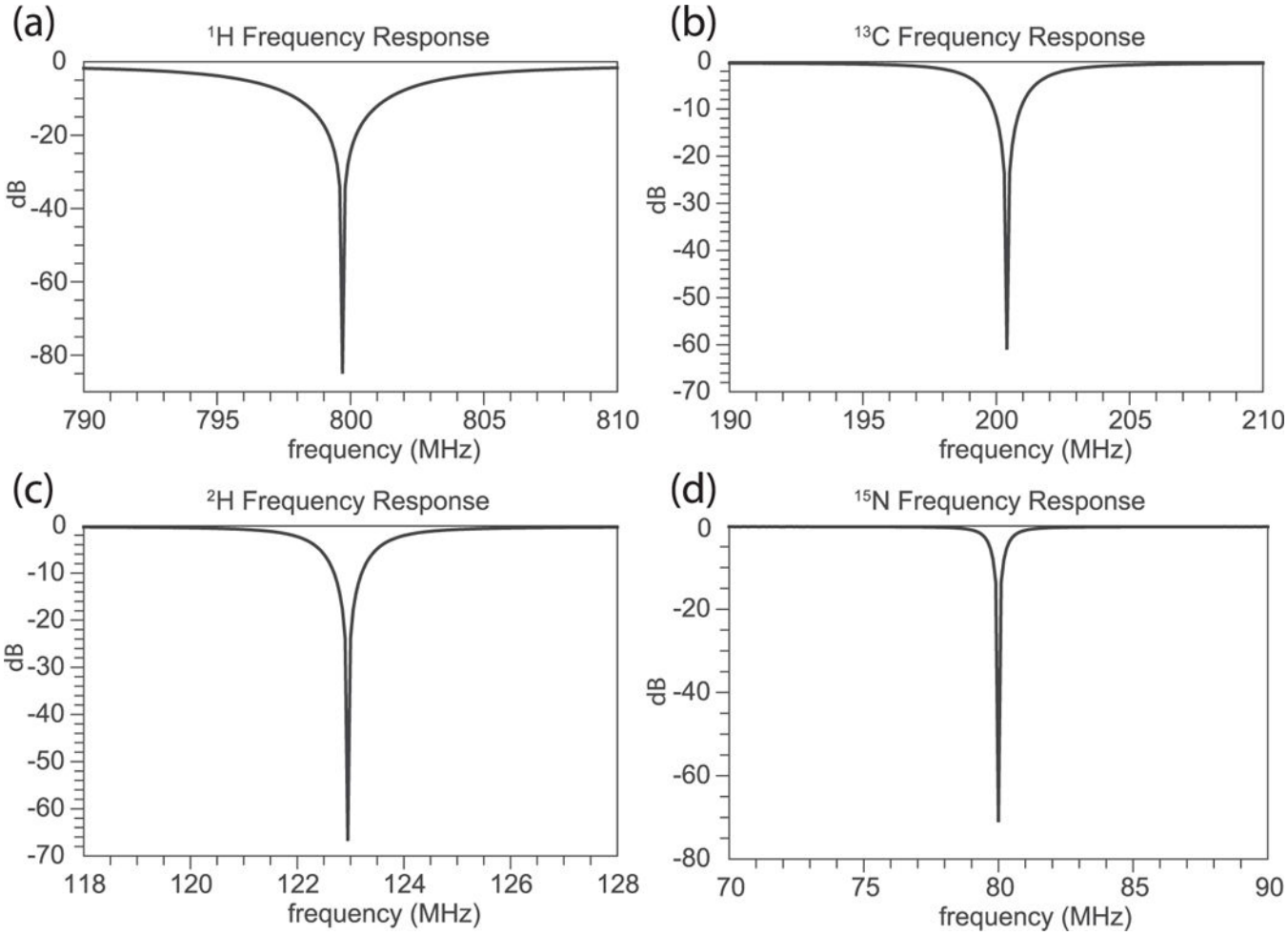

Fig. 6.

Reflectances of the (a) ^{1}H, (b) ^{13}C, (c) ^{2}H, and (d) ^{15}N channels.

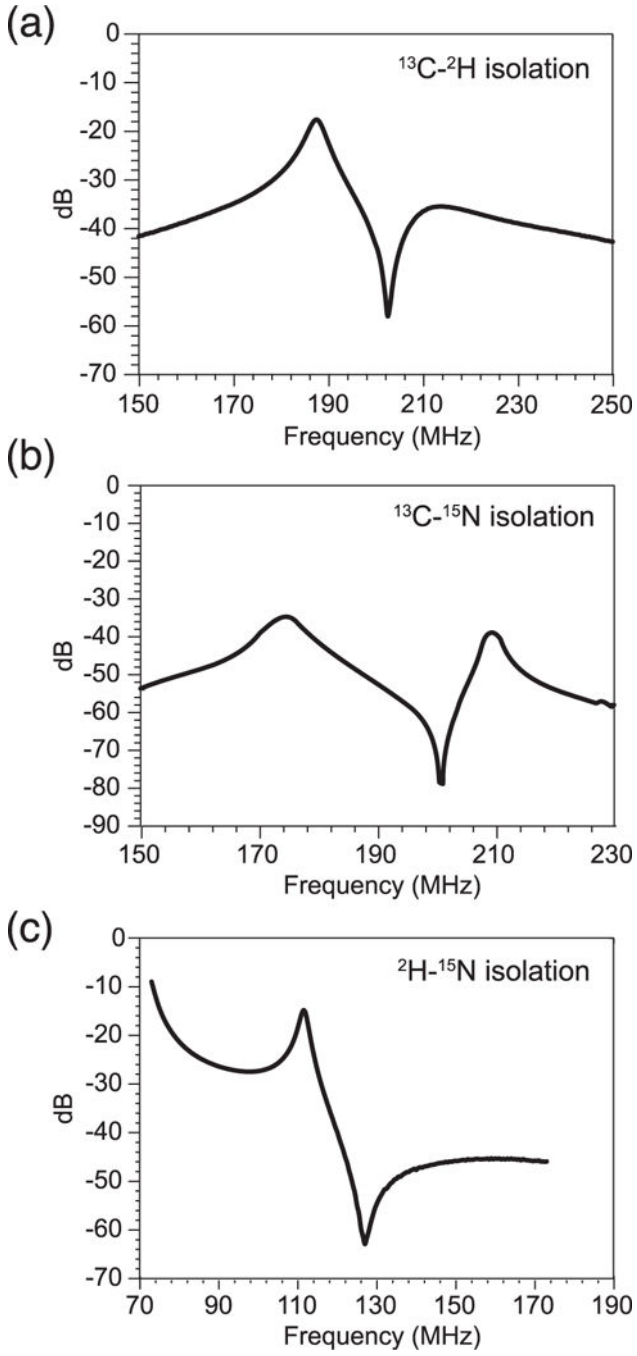

Fig. 7.

Isolation among the channels of the triple-resonance circuit. (a) Output on the ^{13}C channel as the input frequency is swept on the ^{2}H channel. (b) Output on the ^{13}C channel as the input frequency is swept on the ^{15}N channel. (c) Output on the ^{2}H channel as the input frequency is swept on the ^{15}N channel.

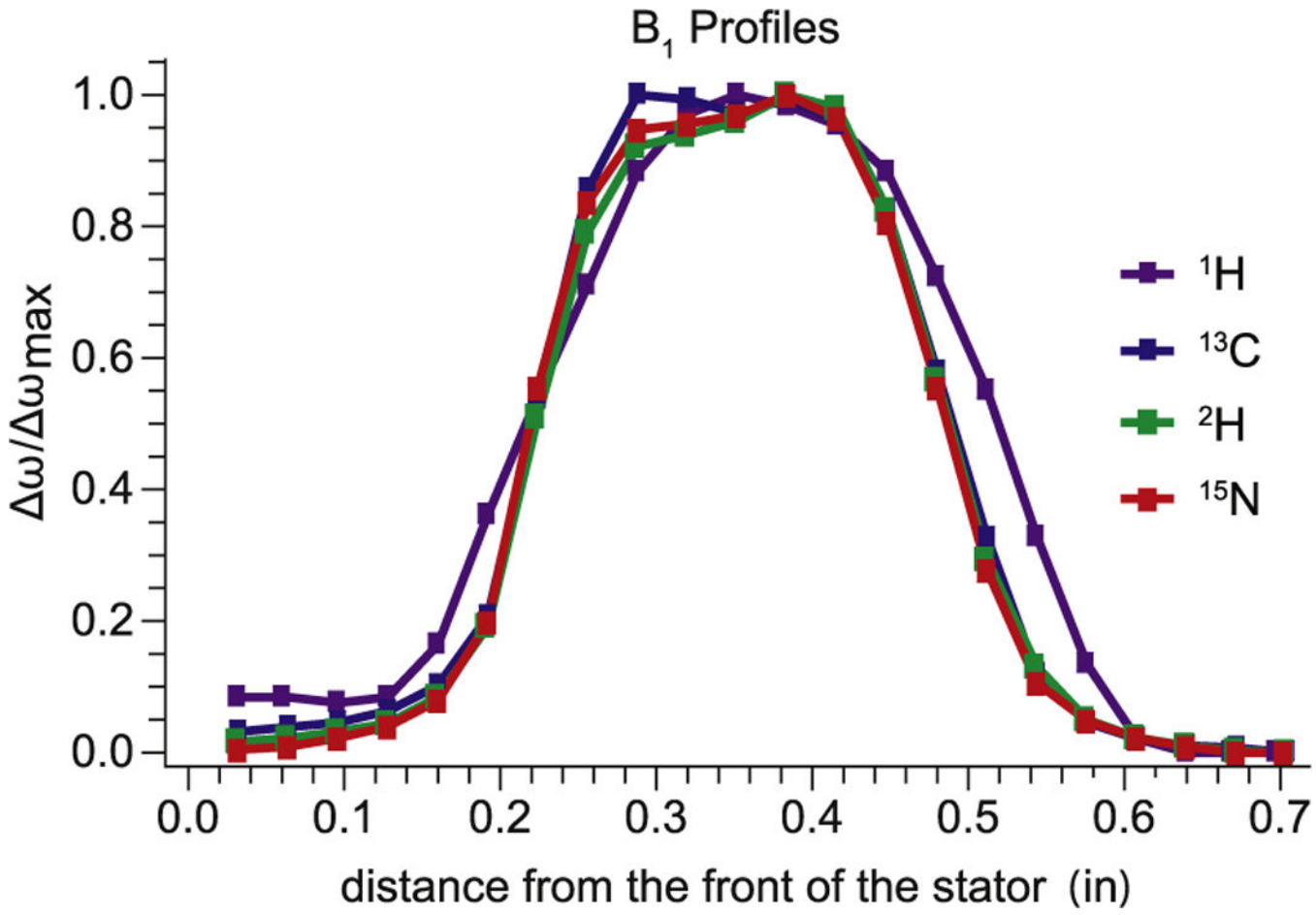

Fig. 8.

Homogeneity plots of the four channels measured with the ball-shift method. The characteristic plateau shape indicates the homogeneous magnetic field region of each channel. The position of the solenoid coil within the outer resonator, and the spacing of its coils, were carefully adjusted to align these homogeneous regions. These measurements were performed with both coils in situ.

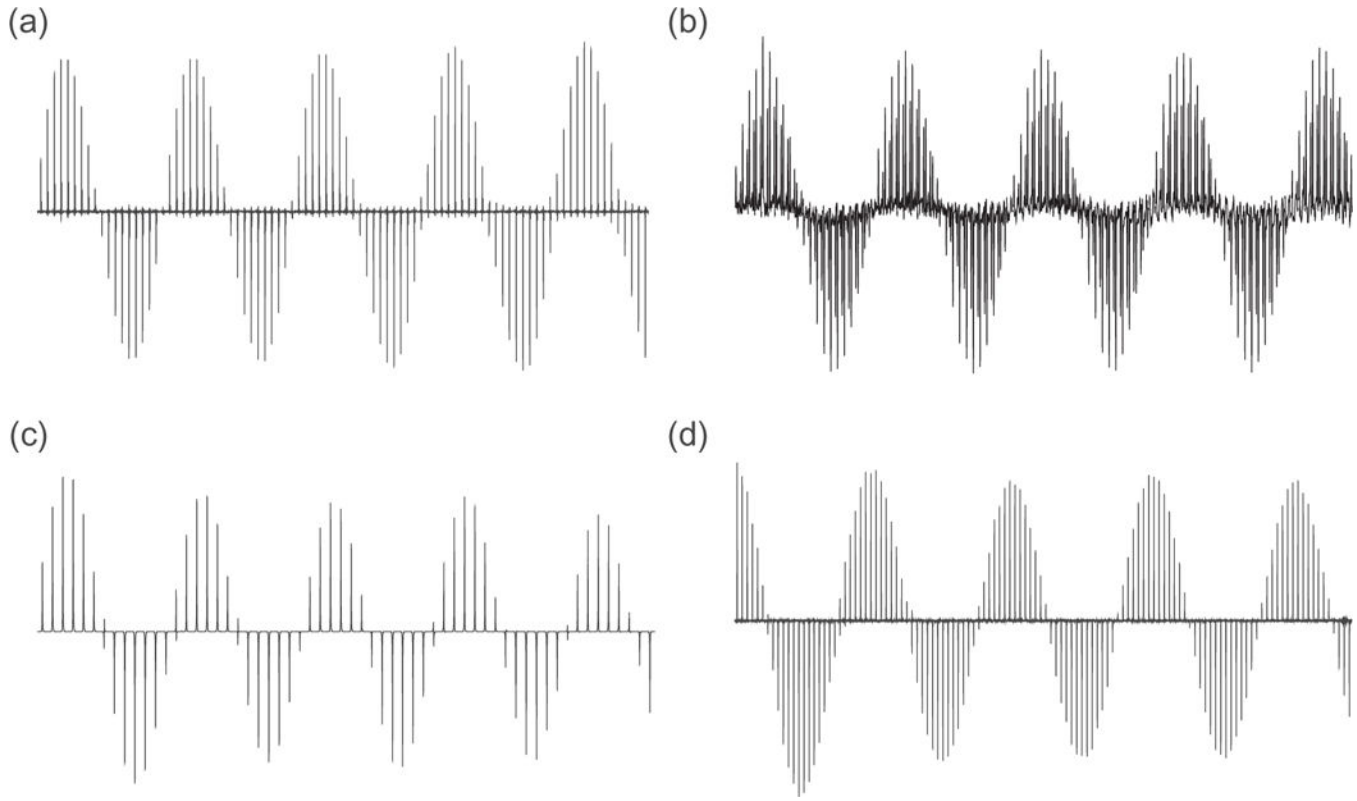

Fig. 9.

Nutation arrays for the four channels, with sample volumes of 20 μL in 3.2 mm rotor. (a) ^{1}H nutation using a one pulse experiment on natural abundance adamantane. (b) ^{13}C nutation using a one pulse experiment on natural abundance adamantane. (c) ^{2}H nutation using a one pulse experiment on 90% D_2O/10% H_2O. (d) ^{15}N nutation using an ^{1}H-^{15}N CP experiment on L-Alanine-^{13}, ^{15}N.

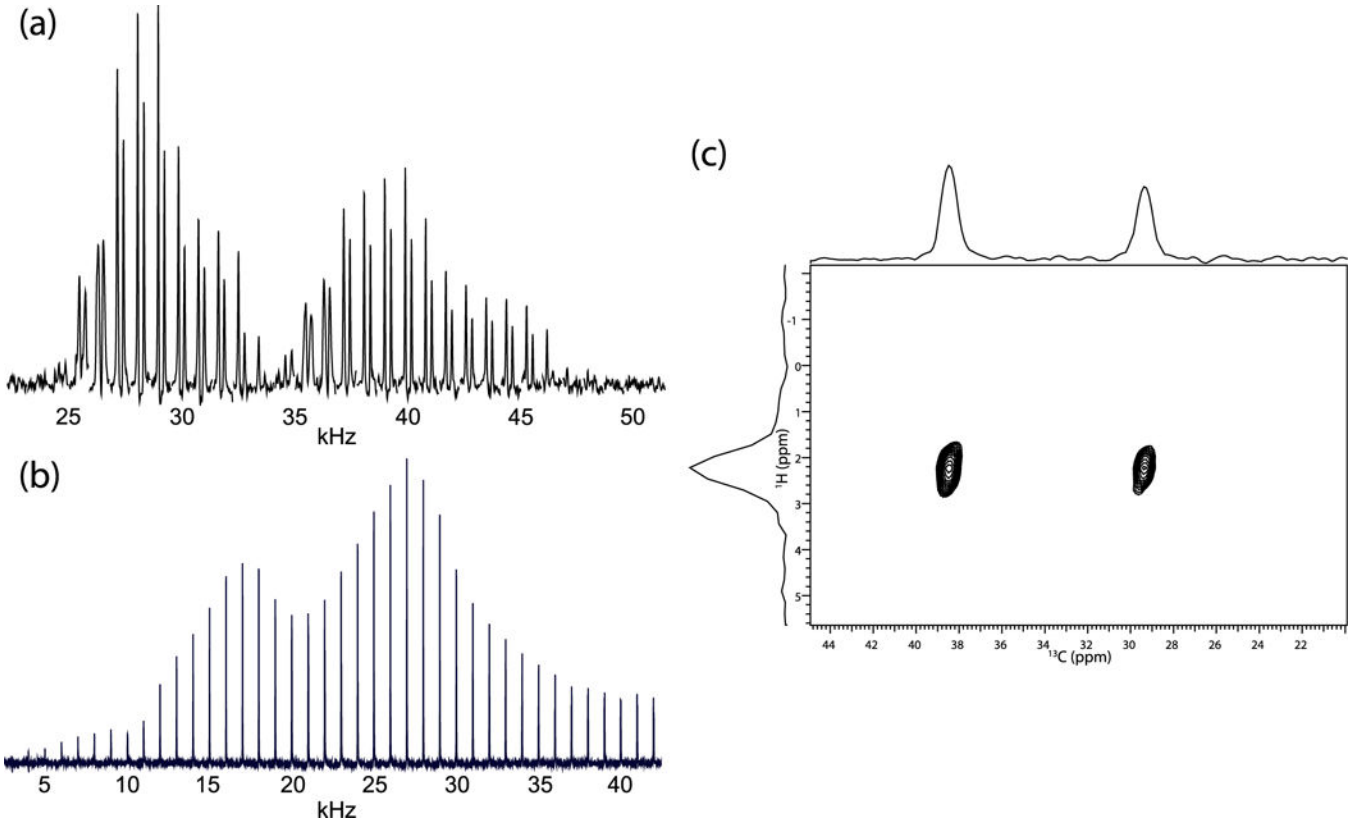

Fig. 10.

(a) ^{1}H-^{13}C cross-polarization match array on adamantane. (b) ^{1}H-^{15}N cross-polarization match array on L-Alanine-^{13}, ^{15}N. (c) ^{1}H-^{13}C HETCOR spectrum of adamantane.

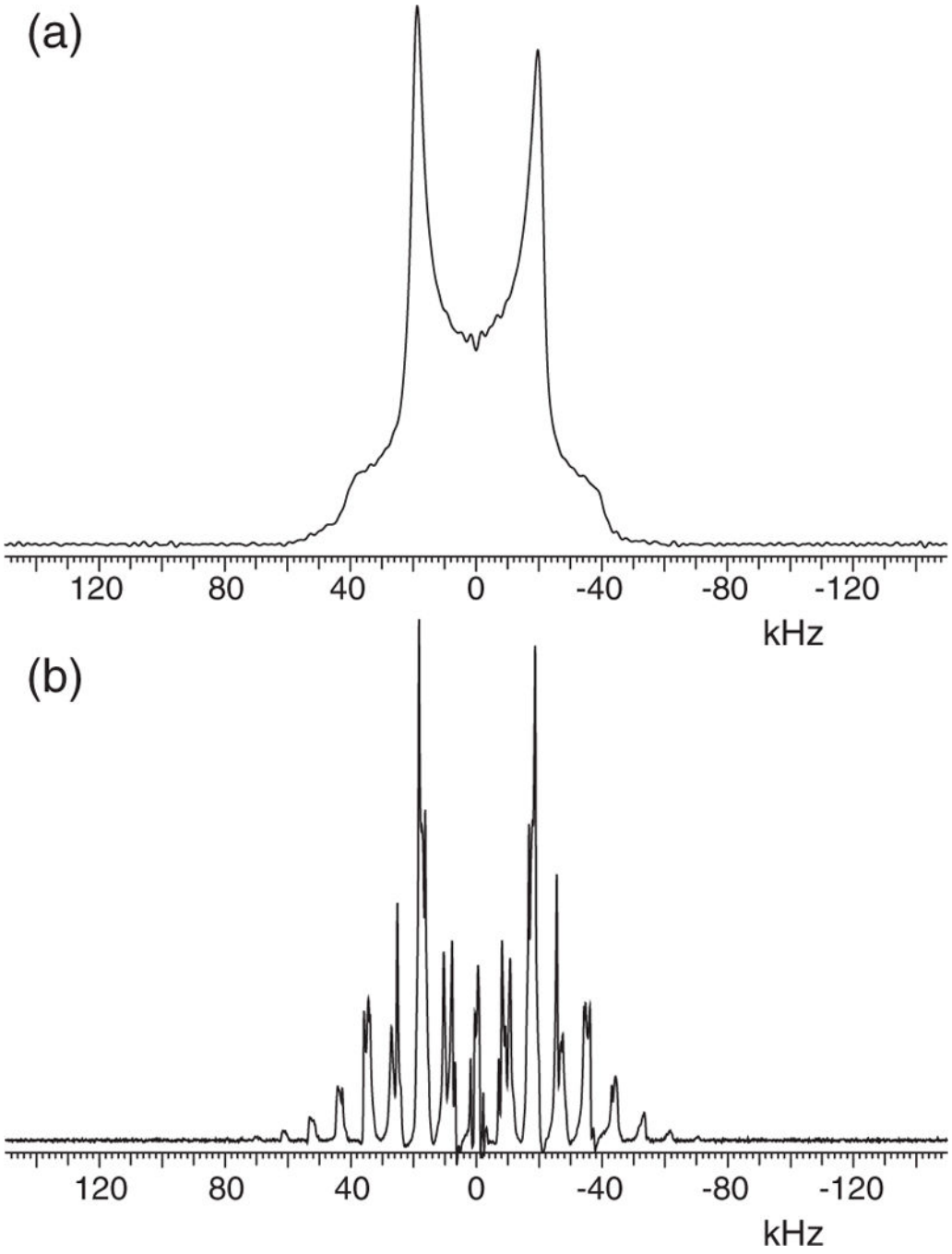

Fig. 11.
^{2}H solid-state echo spectra. (a) Static spectrum. (b) MAS spectrum.

Table 1

Dimensions of channel components (in inches).

Component	^{13}C	^{2}H	^{15}N	^{1}H
Match guide rod (L)	15	17	18.5	15.5
Tune guide rods (L)	20	18.5	20.5	21.75
rf feed (L)	17.5	16.5	19.5	17.25
Tune dielectric (L)	2.125	2	3	1.25
Tune dielectric (ID)	0.25	0.45	0.43	0.3
Lower match conductor (L)	4.75	4.75	4	4.25
Upper match conductor (L)	2.25	1.125	2.5	0.5
Upper match conductor (OD)	0.125	0.185	0.25	0.29
Tune conductor (L)	3.625	3.825	1.75	3.5
Tune conductor (OD)	0.25	0.435	0.435	0.25
Tune conductor (ID)	0.2	0.375	.325	NA

Table 2

Isolation values among the heteronuclear channels.

Channels	Isolation (dB)
^{13}C-^{2}H	−12
^{13}C-^{15}N	−18
^{2}H-^{15}N	−13

Table 3

Power handling and homogeneities of the probe channels

Channel	Power (W)	90°-time (μs)	810°/90°	Q
^{1}H	53.8	4.75	0.992	180
^{13}C	100	5.5	0.923	130
^{2}H	334	3.5	0.755	164
^{15}N	98.6	7	0.883	167